scientific reports

OPEN

Fabrication of polyhedral Cu–Zn oxide nanoparticles by dealloying and anodic oxidation of German silver alloy for photoelectrochemical water splitting

Nour Bahnasawy, Abdussalam M. Elbanna, Mohamed Ramadan & Nageh K. Allam ✉

A significant effort has been dedicated to the synthesis of Cu–Zn oxide nanoparticles as a robust photocathode material for photoelectrochemical water splitting. Cu–Zn oxide nanoparticles were formed by controlled anodization of German silver (Cu–Zn–Ni) alloy in an aqueous electrolyte. Scanning electron microscopy (SEM) demonstrates the dependence of the obtained nanostructures on the anodization time. The X-ray diffraction (XRD) patterns showed the formation of copper oxide (CuO) and zinc oxide (ZnO) nanoparticles with good stability. This was also confirmed by the compositional X-ray photoelectron spectroscopy (XPS) analysis. The obtained polyhedral nanoparticles showed high optical activity with adequate bandgap energy. These optimized nanoparticles achieved boosted photocurrent of − 0.55 mA/cm^2 at − 0.6 V vs. SCE under AM 1.5 illumination, confirming the role of the optimized dealloying and thermal treatment in tuning the photoelectrochemical performance of the material.

Extensive research has been conducted to improve the performance of photoelectrochemical water splitting systems[1–3]. The scarcity of low-cost, earth-abundant, photoactive, and stable photoelectrodes is the challenge in realizing the commercialization of such systems[4]. To this end, earth-abundant metal oxides can be utilized as effective photoelectrodes to attain this purpose[5–7]. Among several metal oxides, copper oxides are considered a class of the best metal oxide semiconductors due to their high absorption over a wide range of the solar spectrum and being cost-effective, non-toxic, and abundant in nature[8–12]. Despite their excellent electronic transport properties, absorption coefficient, and direct bandgap[9–13], copper oxides are unstable, hindering their wide use in aqueous electrolyte-based systems. Hence, more efforts have been devoted to improving their stability, such as coating, doping with several metals and nonmetals[14], annealing treatments[15], and nanostructuring[16]. Still, among those used protocols are severe artifacts[17]. On the contrary, ZnO has high stability but a wide bandgap[18–20], which restricts its absorption to the UV region of the light spectrum. Several efforts were exerted to improve its optical activity, including nanostructuring[21], decoration[22], and doping[20,21], but with limited success.

Moreover, nanoscale materials have a plethora of merits over bulk materials, including the high surface area, enhanced physical properties, and tuned electronic properties[23]. The more surface area, the more active sites are available for reactions to occur. Moreover, the very small size (lower than 10 nm) results in quantum confinement effects that improve the charge carriers separation and transport. In addition, these nanomaterials can be produced in different morphologies, such as tubes, rods, flowers, spheres, and many more, enabling tuned characteristics[24].

Unfortunately, the overall water splitting efficiency is hindered by the sluggish kinetics of the oxygen evolution reaction (OER) at the anode that involves a complex, four-electron/proton transfer process[25]. Over the last few years, RuO$_2$ and IrO$_2$-based materials are considered the benchmark electrocatalysts for OER due to their high electrocatalytic efficiencies and outstanding carrier mobilities. On the other hand, noble platinum (Pt)-based

Energy Materials Laboratory, School of Sciences and Engineering, The American University in Cairo, New Cairo 11835, Egypt. ✉email: nageh.allam@aucegypt.edu

materials are the most efficient electrocatalysts and the benchmarks for the hydrogen evolution reaction (HER) due to lower Tafel slopes and overpotentials. However, the higher cost of those materials limits their widespread applications[26,27]. Hence, exploring alternative low-cost and high-performance water-splitting catalysts is neccessary. As a result, many efforts have been devoted to tune the cost effective transition metal-based materials for use as non-noble metallic catalysts[28]. Specifically, multi-transition metallic alloy electrocatalysts have stimulated great interest in water splitting applications due to their intrinsic electrocatalytic activity and ease of manipulating their electronic structure[29].

To this end, the combination of CuO and ZnO nanostructures has been widely studied in photocatalytic systems with the aim of integrating the complimentary properties of each oxide[30–32]. The CuO–ZnO heterostructures were prepared by a plethora of methods, including electrochemical deposition and radiofrequency magnetron sputtering. However, these techniques require a long processing time, high temperatures, and are costly. Hence, it is of great importance to identify a more straightforward process to fabricate CuO–ZnO heterostructured nanomaterials. To this end, electrochemical anodization is a surface modification technique that is extensively used to create vast nanostructures of several metals and alloys for different applications[7,16,33–35].

Herein, we report on the optimized fabrication of CuO–ZnO heterostructures with controlled morphology via simple anodization of German silver alloy (Cu–Zn–Ni) followed by air annealing. The produced nanoparticles were investigated as photocathodes to split water photoelectrochemically. It is worth noting that this is the first study on the fabrication of photocathode nanocatalysts via the anodization of German silver alloy and their application in water splitting systems. Note that a current density of CuO of − 0.48 mA/cm^2 at 0.473 V vs. RHE was reported, which is lower than ours even at much lower potential[36,37].

Experimental section

Before anodization, the German silver alloy (65% Cu–22% Zn–13% Ni) was mechanically polished with grinding paper to remove the native oxide. Furthermore, three samples were immersed in dilute HCl, then washed with deionized water. After that, the samples were ultrasonicated in ethanol, water, and acetone for 10 min each. The samples were anodized at room temperature under a constant voltage of 4 V for 2, 5, and 8 min in 0.1 M APS (1 mL), 2.5 M NaOH (1 mL), and 48 mL of deionized water. The distance between the two electrodes is fixed at 1.5 cm. The anodized samples were annealed in air at 350 °C for 1 h with a ramping rate of 5 °C/min. The morphology and the composition of the films are illustrated using a Zeiss SEM Ultra 60 FESEM machine with an accelerating voltage of 4 kV. The crystal structure of the annealed sample was determined using a PANalytical X-pert Pro PW3040 MPD X-ray diffractometer via monochromatic radiation (Cu-Kα, λ = 0.15406 nm, 50 mA, 40 kV) in the range of 5°–80° with a glancing angle of 0.5°. The optical characterization of the fabricated photocathode was performed using a Shimadzu UV–Vis diffuse reflectance spectrometer, and their optical band gap energy was calculated using a Tauc plot. The photoelectrochemical analysis was performed in 1.0 M Na$_2$SO$_4$ in a three-electrode cell with an SCE electrode as a reference electrode, platinum as a counter electrode, and the photocathode as the working electrode using Bio-Logic SP 200 potentiostat using a 300 W Ozone-free Xenon lamp under 100 mW/cm^2 illumination equipped with AM 1.5G filter.

Results and discussion

The morphology of the fabricated samples before and after annealing was inspected using FESEM, as presented in Fig. 1. The surface of the as-anodized sample is entirely covered with homogeneous polyhedral nanoparticles, Fig. 1a,c. The polyhedral nanoparticles were achieved upon anodization of the German silver alloy in the aqueous electrolyte containing 0.1 M ammonium persulfate (APS) and 2.5 M NaOH at 4 V for different times. The oxidation of the alloy formed oxide nanoparticles, and the process was accelerated by using the APS oxidant. We believe the oxidation process in sodium hydroxide occurs in a few steps. First, lower metal oxide (e.g., Cu$_2$O) is formed, then oxidized to the higher oxide (e.g., CuO), and finally, metal hydroxide (e.g., Cu(OH)$_2$) covers the outer layer of the oxide structures[38,39]. Moreover, the present persulfate ions in the electrolyte cause pitting of the formed oxide layer leading to the formation of the observed polyhedral nanoparticles[40] The FESEM image of the as-anodized samples reveals a uniform distribution and good interconnectivity of the formed oxide polyhedral nanoparticles. The as-anodized samples were calcined at 350 °C for 1 h in ambient air to dehydrate and complete the conversion of the hydroxide into the corresponding oxide (Fig. 1b)[41]. However, upon annealing, some of the polyhedral nanoparticles tend to agglomerate (Fig. 1d) due to the difference in the thermal expansion coefficient between the film and the substrate[42,43].

To get a better understanding of the composition of the fabricated photocathodes, an XPS analysis was conducted. Figure 2a illustrates the survey spectra of the annealed photocathode, which demonstrate the existence of Cu, Zn, and O peaks. Figure 2b,c show the spectra of Cu 2p and Zn 2p, respectively. The Cu 2p spectrum exhibits two peaks at 932.69 eV and 952.54 eV, attributing to Cu 2p$_{3/2}$ and Cu 2p$_{1/2}$, respectively. The satellite peaks at 941.21 eV, 943.77 eV, and 962.02 eV are related to the bivalent energy state of copper, characteristic of Cu^{2+}[10,12,44,45]. The peaks at 1021.54 and 1044.62 eV correspond to the Zn 2p$_{3/2}$ and Zn 2p$_{1/2}$, respectively. The observed difference between these binding energies was found to be 23.08 eV, confirming the Zn^{2+} oxidation state[46–49]. The peak at 529.75 eV, Fig. 2d, is characteristic of lattice oxygen in metal oxides. Thus, the XPS results support the formation of CuO and ZnO.

Figure 3 shows the XRD pattern of the fabricated photocathode. The peaks observed at 35.43°, 38.85°, 53.30°, 58.03°, 65.61°, 68.16°, and 72.69° can be ascribed to the (002), (111), (020), (202), (022), (220), and (311) planes of monoclinic CuO (JCPDS# 00-041-0254)[50–52]. Moreover, the peaks appeared at 36.23°, 42.12°, 49.39°, and 61.44° can be assigned to the (111), (200), (200), and (220) planes of cubic ZnO (JCPDS# 01-077-0191) (JCPDS# 01-078-46100)[47,53]. The peaks that appeared at 43.09°, 50.15°, and 73.86° can be related to the substrate[54]. Thus,
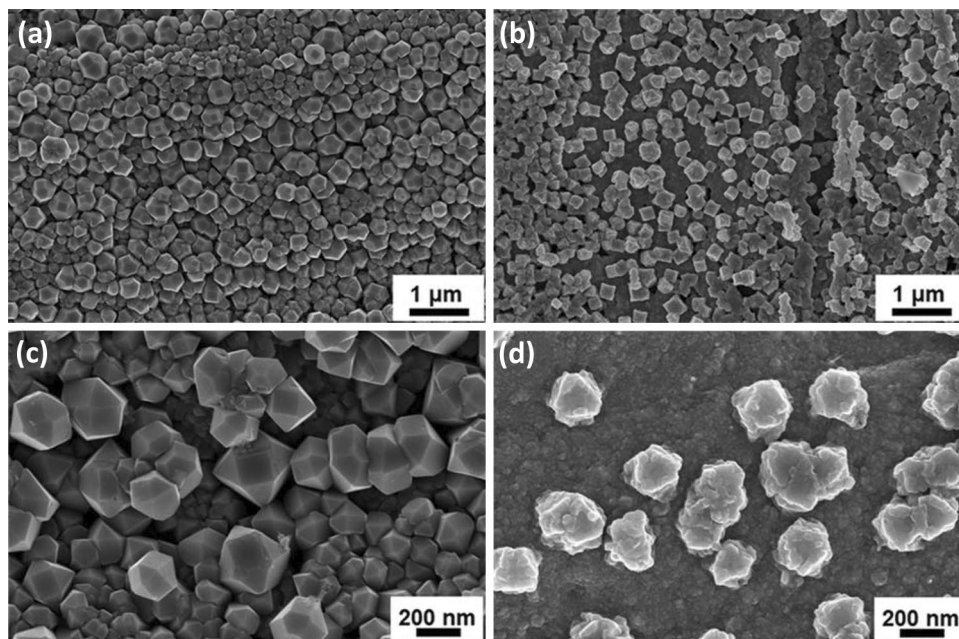
Figure 1. FESEM images of the fabricated photocathodes (**a,c**) before and (**b,d**) after annealing at 350 °C in the air for 1 h.
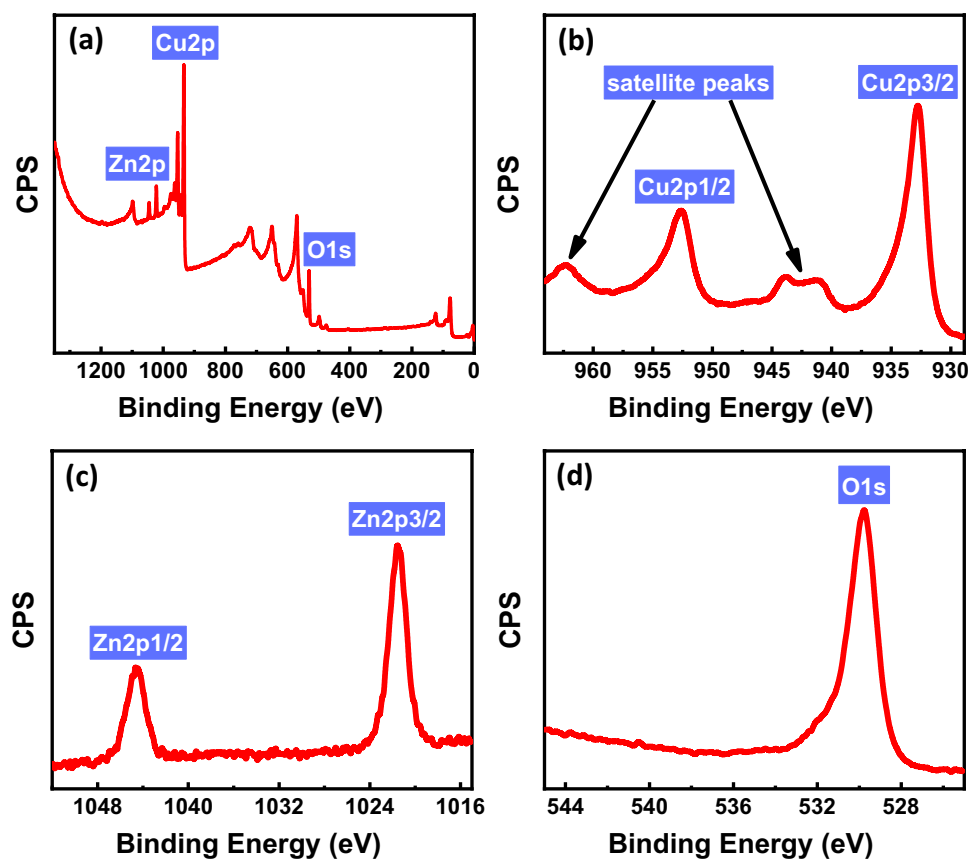

Figure 2. (**a**) XPS survey spectra, high-resolution XPS scans of (**b**) Cu 2p, (**c**) Zn 2p, and (**d**) O 1 s for the fabricated photocathode annealed at 350 °C in the air for 1 h.
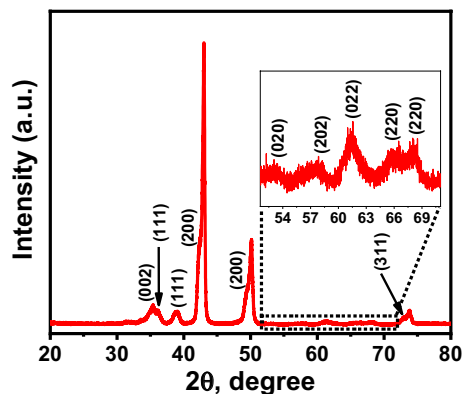
Figure 3. XRD pattern of the fabricated photocathode annealed at 350 °C in the air for 1 h.
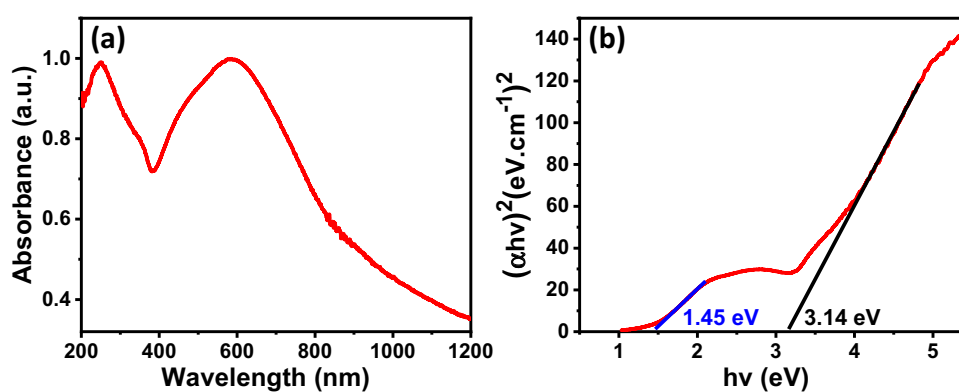

Figure 4. (**a**) UV–Vis absorption spectra and (**b**) Tauc plot of the fabricated photocathode annealed at 350 °C for 1 h in air.

the XRD spectra indicate that the sample's surface is covered by a thin film of mixed CuO and ZnO. The average crystallite sizes (D) of CuO and ZnO nanoparticles were calculated using the Scherrer formula:

$$D = \frac{K\lambda}{\beta \cos\theta} \tag{1}$$

where θ is the Bragg diffraction angle, λ is the X-ray wavelength, and β is the full width at half maximum of the XRD peak existing at a diffraction angle θ. The average crystallite sizes for CuO and ZnO nanoparticles were calculated to be 34.64 and 32.52 nm, respectively[55,56].

The optical activity of the fabricated photocathode was tested using a UV–Vis spectrometer. Figure 4a shows the absorption spectrum of the fabricated photocathode. Two prominent absorption bands were observed at 855 nm and 394 nm, ascribed to the characteristic absorption of CuO and ZnO, respectively[57,58]. To estimate the bandgap energy of the material, Tauc plot was constructed according to Eq. (2):

$$(\alpha h\nu)^n = A\left(h\nu - E_g\right) \tag{2}$$

where α is the absorption coefficient obtained from UV–Vis spectra, $h\nu$ is the photon's energy, A is a constant, E_g is the optical bandgap energy, and n depends on the nature of the transition in a semiconductor. As shown in Fig. 4b, straight lines are determined when $(\alpha h\nu)^2$ is plotted *versus* photon energy ($h\nu$), indicating that the absorption is due to a direct transition ($n = 2$) for both CuO[59,60] and ZnO[61,62]. The bandgap energies of CuO and ZnO were found to be 1.45 eV and 3.14 eV, respectively. These values are in good agreement with those previously reported[63–66].

To photoactivity of the fabricated photocathodes was evaluated in a three-electrode photoelectrochemical cell. Figure 5 shows the linear sweep voltammetry (LSV) of the photocathode in the dark and under illumination. An observed increase in the current density was shown for all samples when exposed to light, as shown in Fig. 5a–c. Eventually, these photo-induced cathodic currents indicate the p-type behavior of copper oxide nanoparticles[67]. The sample anodized for 2 min showed the lowest photocurrent density compared to those counterpart samples prepared by anodization at longer times. This can be ascribed to the lack of active sites that are exposed to light and may indicate the incomplete nanostructuring of the whole surface of the substrate at shorter anodization
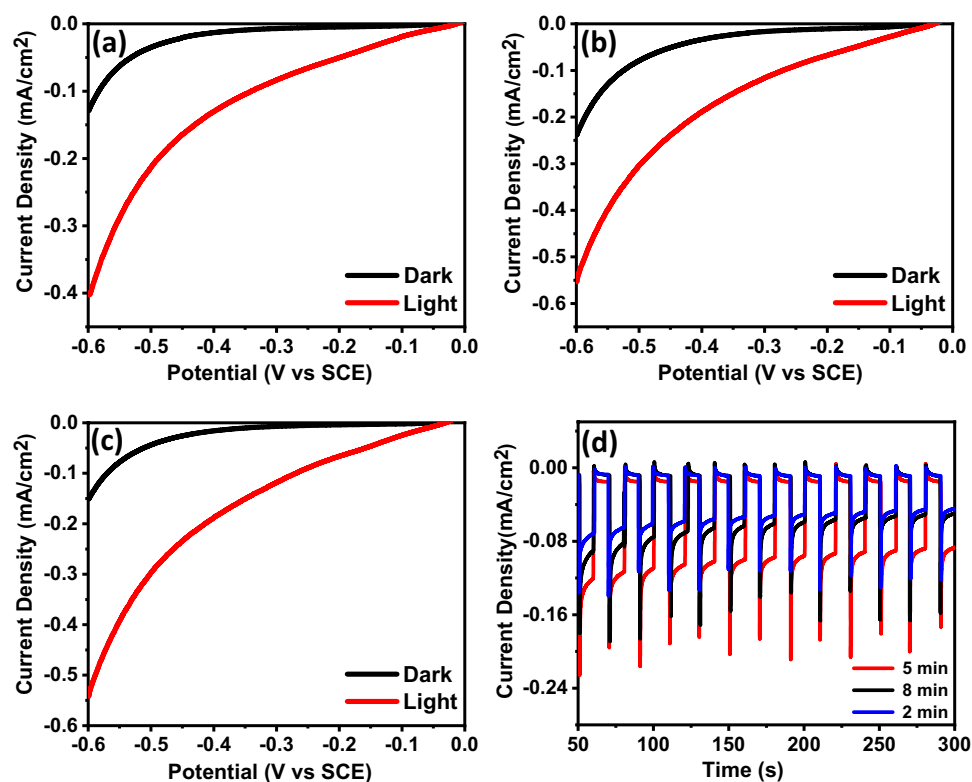
Figure 5. *J–V* and *J–t* curves of annealed Cu–Zn oxide photocathodes that anodized for (**a**) 2 min, (**b**) 5 min, (**c**) 8 min, and (**d**) the transient photocurrent (J–t).

time. However, at 8 min of anodization, the covering on the surface of polyhedral nanoparticles will restrain the entry of sunlight[68,69]. The sample anodized for 5 min showed an increased photocurrent of − 0.55 mA/cm² at − 0.6 V vs. SCE, which can be ascribed to the increased light absorption. Although the sample anodized for 8 min showed approximately the same photocurrent as the sample anodized for 5 min, the dark current was lower.

To examine the photostability of the fabricated photocathodes, the *J–t* curves of the fabricated photocathodes were recorded at a constant potential of − 0.4 V vs. SCE for 300 s under dark and illumination, as shown in Fig. 5d. The sample anodized for 5 min showed the highest photocurrent density, indicating good charge separation and collection compared to other samples. Besides, the samples anodized for 2 and 8 min showed nearly similar photocurrent density. Note that the observed photocurrent decay occurs as a result of the photoreduction of CuO under illumination to form Cu$_2$O and, finally, copper. The samples anodized for 2 min and 8 min showed decay in photocurrent density of 45% and 50% after 300 s, respectively.

On the other hand, the sample anodized for 5 min retrieved better stability with 68% photocurrent retention after 300 s. Hence, the sample anodized for 5 min is considered the best electrode among the other fabricated samples[57]. The photocurrent density of our fabricated electrodes is much higher than those reported for other trimetallic systems for photoelectrochemical water splitting[7,70–74].

Conclusion

In summary, a simple synthesis method of polyhedral Cu–Zn oxide nanoparticles via anodization followed by annealing treatment is demonstrated. The XPS analysis indicated the formation of Cu–Zn-O. Moreover, the XRD analysis confirmed the existence of both CuO and ZnO. The UV–Vis absorption spectra showed the material to have two absorption band edges with corresponding bandgap energies of 1.45 eV and 3.14 eV, in agreement with the materials characterization data. The electrodes showed a photocurrent of − 0.55 mA/cm² at − 0.6 V vs. SCE under AM 1.5 illumination, which is much higher than those reported for other trimetallic systems. Accordingly, this study introduces avenues to design and fabricate stable and photoactive electrodes for photoelectrochemical hydrogen production.

References

1. Navarro, R. M., del Valle, F., Villoria de la Mano, J. A., Álvarez-Galván, M. C. & Fierro, J. L. G. Photocatalytic water splitting under visible light. Concept and catalysts development. *Adv. Chem. Eng.* **36**, 111–143. https://doi.org/10.1016/S0065-2377(09)00404-9 (2009).

2. Allam, N. K., Alamgir, F. & El-Sayed, M. A. Enhanced photoassisted water electrolysis using vertically oriented anodically fabricated Ti– Nb– Zr– O mixed oxide nanotube arrays. *ACS Nano* **4**, 5819–5826 (2010).
3. Badawy, I. M., Elbanna, A. M., Ramadan, M. & Allam, N. K. Propping the electrochemical impedance spectra at different voltages reveals the untapped supercapacitive performance of materials. *Electrochim. Acta* **408**, 139932. https://doi.org/10.1016/j.electacta.2022.139932 (2022).
4. Li, C., He, J., Xiao, Y., Li, Y. & Delaunay, J. J. Earth-abundant Cu-based metal oxide photocathodes for photoelectrochemical water splitting. *Energy Environ. Sci.* **13**, 3269–3306. https://doi.org/10.1039/d0ee02397c (2020).
5. Awad, N. K., Ashour, E. A. & Allam, N. K. Recent advances in the use of metal oxide-based photocathodes for solar fuel production. *J. Renew. Sustain. Energy* **6**, 022702. https://doi.org/10.1063/1.4871899 (2014).
6. Ramadan, M., Abdellah, A. M., Mohamed, S. G. & Allam, N. K. 3D Interconnected binder-free electrospun MnO@C nanofibers for supercapacitor devices. *Sci. Rep.* **8**, 7988. https://doi.org/10.1038/s41598-018-26370-z (2018).
7. Elbanna, A. M. *et al.* Ternary Ti-Mo-Fe nanotubes as efficient photoanodes for solar-assisted water splitting. *J. Phys. Chem. C* **125**, 12504–12517. https://doi.org/10.1021/acs.jpcc.1c01478 (2021).
8. Lu, Y. *et al.* Facile synthesis of graphene-like copper oxide nanofilms with enhanced electrochemical and photocatalytic properties in energy and environmental applications. *ACS Appl. Mater. Interfaces* **7**, 9682–9690. https://doi.org/10.1021/acsami.5b01451 (2015).
9. Khan, M. A., Wahab, Y., Muhammad, R., Tahir, M. & Sakrani, S. Catalyst-free fabrication of novel ZnO/CuO core-Shell nanowires heterojunction: Controlled growth, structural and optoelectronic properties. *Appl. Surf. Sci.* **435**, 718–732. https://doi.org/10.1016/j.apsusc.2017.11.071 (2018).
10. Khan, M. A., Nayan, N., Shadiullah, M. K. & Ahmad, C. F. S. Surface study of CuO nanopetals by advanced nanocharacterization techniques with enhanced optical and catalytic properties. *Nanomaterials* **10**, 1–18. https://doi.org/10.3390/nano10071298 (2020).
11. Hsu, Y. K., Yu, C. H., Lin, H. H., Chen, Y. C. & Lin, Y. G. Template synthesis of copper oxide nanowires for photoelectrochemical hydrogen generation. *J. Electroanal. Chem.* **704**, 19–23. https://doi.org/10.1016/j.jelechem.2013.06.008 (2013).
12. Badawy, I. M., Ismail, A. M., Khedr, G. E., Taha, M. M. & Allam, N. K. Selective electrochemical reduction of CO_2 on compositionally variant bimetallic Cu–Zn electrocatalysts derived from scrap brass alloys. *Sci. Rep.* **12**, 13456 (2022).
13. Liu, C. *et al.* CuO/ZnO heterojunction nanoarrays for enhanced photoelectrochemical water oxidation. *Appl. Surf. Sci.* **469**, 276–282. https://doi.org/10.1016/j.apsusc.2018.11.054 (2019).
14. Mor, G. K. *et al.* Erratum: p-Type Cu-Ti-O Nanotube arrays and their use in self-biased heterojunction photoelectrochemical diodes for hydrogen generation. *Nano Lett.* **8**, 3555. https://doi.org/10.1021/nl8022252 (2008).
15. Paracchino, A., Laporte, V., Sivula, K., Grätzel, M. & Thimsen, E. Highly active oxide photocathode for photoelectrochemical water reduction. *Nat. Mater.* **10**, 456–461. https://doi.org/10.1038/nmat3017 (2011).
16. Allam, N. K. & Grimes, C. A. Electrochemical fabrication of complex copper oxide nanoarchitectures via copper anodization in aqueous and non-aqueous electrolytes. *Mater. Lett.* **65**, 1949–1955. https://doi.org/10.1016/j.matlet.2011.03.105 (2011).
17. Samir, N., Eissa, D. S. & Allam, N. K. Self-assembled growth of vertically aligned ZnO nanorods for light sensing applications. *Mater. Lett.* **137**, 45–48. https://doi.org/10.1016/j.matlet.2014.08.114 (2014).
18. Pietruszka, R. *et al.* New efficient solar cell structures based on zinc oxide nanorods. *Sol. Energy Mater. Sol. Cells* **143**, 99–104. https://doi.org/10.1016/j.solmat.2015.06.042 (2015).
19. Liang, Y. C. & Chang, C. W. Improvement of ethanol gas-sensing responses of $ZnO-WO_3$ composite nanorods through annealing induced local phase transformation. *Nanomaterials* https://doi.org/10.3390/nano9050669 (2019).
20. Hatch, S. M., Briscoe, J. & Dunn, S. A self-powered ZnO-nanorod/CuSCN UV photodetector exhibiting rapid response. *Adv. Mater.* **25**, 867–871. https://doi.org/10.1002/adma.201204488 (2013).
21. Hassan, N. K., Hashim, M. R. & Allam, N. K. ZnO nano-tetrapod photoanodes for enhanced solar-driven water splitting. *Chem. Phys. Lett.* **549**, 62–66 (2012).
22. Shaheen, B. S., Salem, H. G., El-Sayed, M. A. & Allam, N. K. Thermal/electrochemical growth and characterization of one-dimensional ZnO/TiO_2 hybrid nanoelectrodes for solar fuel production. *J. Phys. Chem. C* **117**, 18502–18509 (2013).
23. Guo, D., Xie, G. & Luo, J. Mechanical properties of nanoparticles: Basics and applications. *J. Phys. D Appl. Phys.* https://doi.org/10.1088/0022-3727/47/1/013001 (2014).
24. Rani, A. *et al.* A review on the progress of nanostructure materials for energy harnessing and environmental remediation. *J. Nanostruct. Chem.* **8**, 255–291. https://doi.org/10.1007/s40097-018-0278-1 (2018).
25. Duan, Y. *et al.* Scaled-up synthesis of amorphous NiFeMo oxides and their rapid surface reconstruction for superior oxygen evolution catalysis. *Angew. Chem.* **131**, 15919–15924. https://doi.org/10.1002/ange.201909939 (2019).
26. Nong, H. N. *et al.* Oxide-supported IrNiOx core-shell particles as efficient, cost-effective, and stable catalysts for electrochemical water splitting. *Angew. Chem. Int. Ed.* **54**, 2975–2979. https://doi.org/10.1002/anie.201411072 (2015).
27. Zhang, F. *et al.* RuCo alloy bimodal nanoparticles embedded in N-doped carbon: A superior pH-universal electrocatalyst outperforms benchmark Pt for the hydrogen evolution reaction. *J. Mater. Chem. A* **8**, 12810–12820. https://doi.org/10.1039/d0ta04491a (2020).
28. Yan, S., Zhong, M., Wang, C. & Lu, X. Amorphous aerogel of trimetallic FeCoNi alloy for highly efficient oxygen evolution. *Chem. Eng. J.* https://doi.org/10.1016/j.cej.2021.132955 (2022).
29. Zhu, K., Zhu, X. & Yang, W. In-situ-Methoden zur Charakterisierung elektrochemischer NiFe-Sauerstoffentwicklungskatalysatoren. *Angew. Chem.* **131**, 1264–1277. https://doi.org/10.1002/ange.201802923 (2019).
30. Kim, S. *et al.* Synthesis of vertically conformal ZnO/CuO core-shell nanowire arrays by electrophoresis-assisted electroless deposition. *J. Phys. Chem. C* **118**, 7377–7385. https://doi.org/10.1021/jp410293j (2014).
31. Pal, S., Maiti, S., Maiti, U. N. & Chattopadhyay, K. K. Low temperature solution processed ZnO/CuO heterojunction photocatalyst for visible light induced photo-degradation of organic pollutants. *CrystEngComm* **17**, 1464–1476. https://doi.org/10.1039/c4ce02159b (2015).
32. Mansournia, M. & Ghaderi, L. CuO@ZnO core-shell nanocomposites: Novel hydrothermal synthesis and enhancement in photocatalytic property. *J. Alloy. Compd.* **691**, 171–177. https://doi.org/10.1016/j.jallcom.2016.08.267 (2017).
33. Allam, N. K. & El-Sayed, M. A. Photoelectrochemical water oxidation characteristics of anodically fabricated TiO_2 nanotube arrays: Structural and optical properties. *J. Phys. Chem. C* **114**, 12024–12029. https://doi.org/10.1021/jp1037014 (2010).
34. Allam, N. K. & Grimes, C. A. Formation of vertically oriented TiO_2 nanotube arrays using a fluoride free HCl aqueous electrolyte. *J. Phys. Chem. C* **111**, 13028–13032. https://doi.org/10.1021/jp073924i (2007).
35. Lockman, Z., Ismail, S., Sreekantan, S., Schmidt-Mende, L. & MacManus-Driscoll, J. L. The rapid growth of 3 μm long titania nanotubes by anodization of titanium in a neutral electrochemical bath. *Nanotechnology* https://doi.org/10.1088/0957-4484/21/5/055601 (2010).
36. Xing, H. *et al.* Exposing the photocorrosion mechanism and control strategies of a CuO photocathode. *Inorg. Chem. Front.* **6**, 2488–2499. https://doi.org/10.1039/c9qi00780f (2019).
37. Siavash Moakhar, R. *et al.* Photoelectrochemical water-splitting using CuO-based electrodes for hydrogen production: A review. *Adv. Mater.* https://doi.org/10.1002/adma.202007285 (2021).
38. Stepniowski, W. J. & Misiolek, W. Z. Review of fabrication methods, physical properties, and applications of nanostructured copper oxides formed via electrochemical oxidation. *Nanomaterials* **8**, 379. https://doi.org/10.3390/NANO8060379 (2018).

39. Wu, J. *et al.* Nano-scale oxidation of copper in aqueous solution. *Electrochem. Commun.* **26**, 21–24. https://doi.org/10.1016/J.ELECOM.2012.09.042 (2013).

40. Kar, P. *et al.* Anodic copper oxide nanowire and nanopore arrays with mixed phase content: Synthesis, characterization and optical limiting response. *J. Phys. Commun.* https://doi.org/10.1088/2399-6528/aa93a4 (2017).

41. Zhang, Z. & Wang, P. Highly stable copper oxide composite as an effective photocathode for water splitting via a facile electrochemical synthesis strategy. *J. Mater. Chem.* **22**, 2456–2464. https://doi.org/10.1039/C1JM14478B (2012).

42. Umar, M. *et al.* Morphological and stoichiometric optimization of Cu_2O thin films by deposition conditions and post-growth annealing. *Thin Solid Films* **732**, 138763. https://doi.org/10.1016/J.TSF.2021.138763 (2021).

43. Messier, R. Toward quantification of thin film morphology. *J. Vac. Sci. Technol. A Vac. Surf. Films* **4**, 490. https://doi.org/10.1116/1.573866 (1998).

44. Navale, Y. H., Navale, S. T., Chougule, M. A., Ramgir, N. S. & Patil, V. B. NO_2 gas sensing properties of heterostructural CuO nanoparticles/ZnO nanorods. *J. Mater. Sci. Mater. Electron.* **32**, 18178–18191. https://doi.org/10.1007/s10854-021-06360-0 (2021).

45. Kilic, B. *et al.* Interfacial engineering of CuO nanorod/ZnO nanowire hybrid nanostructure photoanode in dye-sensitized solar cell. *J. Nanopart. Res.* https://doi.org/10.1007/s11051-017-4103-4 (2018).

46. Li, J. *et al.* CuO/ZnO heterojunction nanorod arrays prepared by photochemical method with improved uv detecting performance. *Nanomaterials* https://doi.org/10.3390/nano9050790 (2019).

47. Eissa, D. S., El-Hagar, S. S., Ashour, E. A. & Allam, N. K. Electrochemical nano-patterning of brass for stable and visible light-induced photoelectrochemical water splitting. *Int. J. Hydrogen Energy* **44**, 14588–14595. https://doi.org/10.1016/j.ijhydene.2019.04.071 (2019).

48. Ahmad, R. *et al.* Highly efficient non-enzymatic glucose sensor based on CuO modified vertically-grown ZnO nanorods on electrode. *Sci. Rep.* https://doi.org/10.1038/s41598-017-06064-8 (2017).

49. Vuong, N. M., Chinh, N. D., Huy, B. T. & Lee, Y. I. CuO-decorated ZnO hierarchical nanostructures as efficient and established sensing materials for H2S gas sensors. *Sci. Rep.* https://doi.org/10.1038/srep26736 (2016).

50. Xu, Z. *et al.* Fabrication and sterilization characteristics of visible light photocatalyst of CuO/ZrO_2/CB/Coal-Tar-Pitch-SAC. *Coatings* https://doi.org/10.3390/coatings11070816 (2021).

51. Goyal, C. P. *et al.* Effect of Zn doping in CuO octahedral crystals towards structural, optical, and gas sensing properties. *Crystals (Basel)* https://doi.org/10.3390/cryst10030188 (2020).

52. Dhaouadi, H., Kouass, S. & Touati, F. Synthesis, structure and optical properties of x(CuO)/(1−x)Ni(OH)2 [x = 0, 0.1 and 0.3] nanocomposites. *Ceram. Int.* **40**, 7823–7827. https://doi.org/10.1016/j.ceramint.2013.12.126 (2014).

53. Xaba, T., Moloto, M. J. & Moloto, N. Bis(2-hydroxy-1-naphthaldehydato)zinc(II) as a precursor for the preparation of ZnO thin films through aerosol-assisted chemical vapour deposition. *Thin Solid Films* **670**, 99–104. https://doi.org/10.1016/j.tsf.2018.12.018 (2019).

54. Awad, N. K., Ashour, E. A., Fouda, A. S. & Allam, N. K. Effect of alloying elements on the electrochemical behavior of Cu-Ni-Zn ternary system in sulfide-polluted saltwater. *Appl. Surf. Sci.* **307**, 621–630. https://doi.org/10.1016/j.apsusc.2014.04.087 (2014).

55. Singh, I. & Bedi, R. K. Studies and correlation among the structural, electrical and gas response properties of aerosol spray deposited self assembled nanocrystalline CuO. *Appl. Surf. Sci.* **257**, 7592–7599. https://doi.org/10.1016/j.apsusc.2011.03.133 (2011).

56. Raja, K., Ramesh, P. S. & Geetha, D. Structural, FTIR and photoluminescence studies of Fe doped ZnO nanopowder by co-precipitation method. *Spectrochim. Acta Part A Mol. Biomol. Spectroscopy* **131**, 183–188. https://doi.org/10.1016/j.saa.2014.03.047 (2014).

57. Banerjee, S., Myung, Y., Raman, S. & Banerjee, P. Direct growth of flexible and scalable photocathodes from α-brass substrates. *ACS Sustain. Chem. Eng.* **3**, 3197–3204. https://doi.org/10.1021/acssuschemeng.5b01226 (2015).

58. Yang, Q., Tang, K., Zuo, J. & Qian, Y. Synthesis and luminescent property of single-crystal ZnO nanobelts by a simple low temperature evaporation route. *Appl. Phys. A Mater. Sci. Process.* **79**, 1847–1851. https://doi.org/10.1007/s00339-004-2939-9 (2004).

59. Chiang, C. Y. *et al.* Copper oxide nanoparticle made by flame spray pyrolysis for photoelectrochemical water splitting—Part II. Photoelectrochemical study. *Int. J. Hydrogen Energy* **36**, 15519–15526. https://doi.org/10.1016/j.ijhydene.2011.09.041 (2011).

60. Chiang, C. Y., Chang, M. H., Liu, H. S., Tai, C. Y. & Ehrman, S. Process intensification in the production of photocatalysts for solar hydrogen generation. *Ind. Eng. Chem. Res.* **51**, 5207–5215. https://doi.org/10.1021/ie202522g (2012).

61. Balgude, S. D., Sethi, Y. A., Kale, B. B., Amalnerkar, D. P. & Adhyapak, P. V. ZnO decorated Sn_3O_4 nanosheet nano-heterostructure: A stable photocatalyst for water splitting and dye degradation under natural sunlight. *RSC Adv.* **9**, 10289–10296. https://doi.org/10.1039/c9ra00788a (2019).

62. Basnet, P., Samanta, D., Inakhunbi Chanu, T., Mukherjee, J. & Chatterjee, S. Assessment of synthesis approaches for tuning the photocatalytic property of ZnO nanoparticles. *SN Appl. Sci.* https://doi.org/10.1007/s42452-019-0642-x (2019).

63. Zhang, J. *et al.* Tunable fabrication of CuO nanoplates on ZnO nanorods: Heterostructure formation by photodeposition for enhanced photocatalytic activity. *Eur. J. Inorg. Chem.* **2019**, 2654–2660. https://doi.org/10.1002/ejic.201900401 (2019).

64. Nguyen, D. T. *et al.* Experimental and numerical study on photocatalytic activity of the ZnO nanorods/CuO composite film. *Sci. Rep.* https://doi.org/10.1038/s41598-020-64784-w (2020).

65. Oliveira, M. C. *et al.* Connecting theory with experiment to understand the photocatalytic activity of CuO–ZnO heterostructure. *Ceram. Int.* **46**, 9446–9454. https://doi.org/10.1016/j.ceramint.2019.12.205 (2020).

66. Zhu, L. *et al.* Synthesis of the 0D/3D CuO/ZnO heterojunction with enhanced photocatalytic activity. *J. Phys. Chem. C* **122**, 9531–9539. https://doi.org/10.1021/acs.jpcc.8b01933 (2018).

67. Wang, P., Wen, X., Amal, R. & Ng, Y. H. Introducing a protective interlayer of TiO_2 in Cu_2O-CuO heterojunction thin film as a highly stable visible light photocathode. *RSC Adv.* **5**, 5231–5236. https://doi.org/10.1039/c4ra13464h (2015).

68. Han, J., Zong, X., Zhou, X. & Li, C. Cu_2O/CuO photocathode with improved stability for photoelectrochemical water reduction. *RSC Adv.* **5**, 10790–10794. https://doi.org/10.1039/c4ra13896a (2015).

69. Singh, D. P., Neti, N. R., Sinha, A. S. K. & Srivastava, O. N. Growth of different nanostructures of Cu_2O (nanothreads, nanowires, and nanocubes) by simple electrolysis based oxidation of copper. *J. Phys. Chem. C* **111**, 1638–1645. https://doi.org/10.1021/jp0657179 (2007).

70. Song, A. *et al.* Elucidating the optical, electronic, and photoelectrochemical properties of p-type copper vanadate (p-$Cu_5V_2O_{10}$) photocathodes. *J. Mater. Chem. A* **8**, 12538–12547. https://doi.org/10.1039/d0ta04250a (2020).

71. Yu, J. *et al.* Photogenerated electron reservoir in hetero-p-n CuO-ZnO nanocomposite device for visible-light-driven photocatalytic reduction of aqueous Cr(vi). *J. Mater. Chem. A* **3**, 1199–1207. https://doi.org/10.1039/c4ta04526b (2015).

72. Juan, Y. M. *et al.* Electron field emitters made of 3-D CuO nanowires on flexible silicon substrate fabricated by heating Cu rods with through silicon: Via process. *RSC Adv.* **6**, 47292–47297. https://doi.org/10.1039/c6ra07781a (2016).

73. Patel, P. P. *et al.* Nitrogen and cobalt co-doped zinc oxide nanowires—viable photoanodes for hydrogen generation via photoelectrochemical water splitting. *J. Power Sources* **299**, 11–24. https://doi.org/10.1016/j.jpowsour.2015.08.027 (2015).

74. Wang, M. *et al.* N doping to ZnO nanorods for photoelectrochemical water splitting under visible light: Engineered impurity distribution and terraced band structure. *Sci. Rep.* **5**, 1–13. https://doi.org/10.1038/srep12925 (2015).

Competing interests

The authors declare no competing interests as defined by Nature Research, or other interests that might be perceived to influence the results and/or discussion reported in this paper.

Additional information

Correspondence and requests for materials should be addressed to N.K.A.

Reprints and permissions information is available at www.nature.com/reprints.

Publisher's note Springer Nature remains neutral with regard to jurisdictional claims in published maps and institutional affiliations.